Evidence for the Dipole Nature of the Low-Energy γ Enhancement in ^{56}Fe

A. C. Larsen,[1,*] N. Blasi,[2] A. Bracco,[2,3] F. Camera,[2,3] T. K. Eriksen,[1] A. Görgen,[1] M. Guttormsen,[1] T. W. Hagen,[1] S. Leoni,[2,3] B. Million,[2] H. T. Nyhus,[1] T. Renstrøm,[1] S. J. Rose,[1] I. E. Ruud,[1] S. Siem,[1] T. Tornyi,[1,4] G. M. Tveten,[1] A. V. Voinov,[5] and M. Wiedeking[6]

[1]*Department of Physics, University of Oslo, N-0316 Oslo, Norway*
[2]*INFN, Sezione di Milano, I-20133 Milano, Italy*
[3]*Dipartimento di Fisica, University of Milano, I-20122 Milano, Italy*
[4]*Institute of Nuclear Research, MTA ATOMKI, H-4026 Debrecen, Hungary*
[5]*Department of Physics and Astronomy, Ohio University, Athens, Ohio 45701, USA*
[6]*iThemba LABS, Post Office Box 722, 7129 Somerset West, South Africa*

(Received 14 October 2013; published 11 December 2013)

The γ-ray strength function of ^{56}Fe has been measured from proton-γ coincidences for excitation energies up to ≈ 11 MeV. The low-energy enhancement in the γ-ray strength function, which was first discovered in the $(^3\mathrm{He}, \alpha\gamma)^{56}$Fe reaction, is confirmed with the $(p, p'\gamma)^{56}$Fe experiment reported here. Angular distributions of the γ rays give for the first time evidence that the enhancement is dominated by dipole transitions.

DOI: 10.1103/PhysRevLett.111.242504 PACS numbers: 25.20.Lj, 24.30.Gd, 27.40.+z

Atomic nuclei are microscopic systems governed by the laws of quantum mechanics. To understand such systems, detailed studies of the accessible quantum-energy levels and their decay properties are vital. The γ-ray strength function (γSF) is a measure of the average, reduced γ-decay probability of the nucleus and is considered a fruitful concept at high excitation energies where the level spacing is small (the quasicontinuum region).

Structures in the γSF provide information on the underlying nuclear dynamics and degrees of freedom, such as the $M1$ scissors mode [1–3] and the giant electric dipole resonance (GDR) [4]. The γSF is also indispensable for predicting reaction cross sections for the astrophysical nucleosynthesis. Specifically, when there is no $(n, \gamma) - (\gamma, n)$ equilibrium, the shape of the γSF in the vicinity of the neutron threshold plays a crucial role for the (n, γ) reaction rates relevant for the rapid neutron-capture process (r process) [5,6].

An enhancement in the γSF for γ energies below ≈ 4 MeV has been discovered in several fp shells and medium-mass nuclei using the Oslo method, such as ^{56,57}Fe [7] and $^{93-98}$Mo [8]. Recently, the low-energy enhancement (hereby denoted as *upbend*) was confirmed in a $(d, p\gamma)^{95}$Mo experiment [9], using a different detector setup and a model-independent method to extract the γSF. The upbend could induce an increase of up to 2 orders of magnitude in the (n, γ) reaction rates in very neutron-rich isotopes [10]. Depending on the actual conditions at the astrophysical r-process site, this could be of great importance for the r process [10].

Despite the potentially crucial role of the upbend for astrophysics applications, its extent and origin remain largely unknown. In particular, the physical mechanism causing the upbend is not understood, mainly because information on the multipolarity and electromagnetic character is lacking. Only for ^{60}Ni are there data indicating that the upbend is due to $M1$ transitions [11]. However, ^{60}Ni might be a special case with only positive-parity states below excitation energies of ≈ 4.5 MeV. Up to now, data on Fe isotopes are inconclusive regarding the radiation type; neither $E1$, $M1$, nor $E2$ radiation could be excluded (see Fig. 3 in Ref. [7]).

Recent theoretical works on the upbend suggest that it is of $E1$ nature and due to transitions in the single-quasiparticle continuum [12] or of $M1$ type and caused by a reorientation of high-j neutron and proton spins [13]. Apart from the single-particle picture, one could also imagine that strong collective transitions might cause such an enhancement, for example, rotational ($E2$) or vibrational ($E3$) transitions in the quasicontinuum.

In this Letter, we show new data on the γSF of ^{56}Fe. The present data set from the inelastic-scattering reaction $^{56}\mathrm{Fe}(p, p'\gamma)^{56}$Fe yielded high statistics and allowed for a detailed analysis of the γ-ray angular distributions. We present here for the first time results on the multipolarity of the upbend. To our knowledge, this is also the first time where the angular-distribution analyzing tool has been applied to primary γ transitions with a broad distribution of energies at high excitation energies.

The experiment was performed at the Oslo Cyclotron Laboratory (OCL), using a 16-MeV proton beam with intensity ≈ 0.5 nA hitting a self-supporting target of 99.9% enriched ^{56}Fe with mass thickness of 2 mg/cm^2. Accumulating time was ≈ 85 h. The charged ejectiles were measured with the Silicon Ring (SiRi) particle-detector system [14] and the γ rays with the CACTUS array [15]. The SiRi system consists of eight $\Delta E - E$ telescopes, where the front detector is segmented into eight

strips ($\Delta\theta = 2°$), covering scattering angles between 40° and 54°. In total, SiRi has a solid-angle coverage of $\approx 6\%$. Using the $\Delta E - E$ technique, each charged-particle species was identified and a gate was set on the outgoing protons. From the reaction kinematics, the proton energy was converted into excitation energy in the residual nucleus.

In this experiment, the CACTUS array contained 22 collimated $5'' \times 5''$ NaI:Tl detectors, and six collimated $3.5'' \times 8''$ $LaBr_3$:Ce detectors [16,17] from the Milano HECTOR$^+$ array. At the front of the crystals, the conically shaped lead collimators have a radius of 3.5 cm, and the distance to the target is 22 cm, yielding an internal semi-angle of 9°. The NaI detectors were placed in the CACTUS frame with six different angles θ with respect to the beam axis: 37.4°, 63.4°, 79.3°, 100.7°, 116.6°, and 142.6°, while the $LaBr_3$ crystals covered four angles: 63.4°, 79.3°, 100.7°, and 116.6°.

The γ spectra were unfolded using the technique described in Ref. [18], but with new response functions from γ lines of excited states in ^{13}C, ^{16,17}O, ^{28}Si, and ^{56,57}Fe populated with various inelastic-scattering and transfer reactions. Furthermore, the distribution of the primary γ rays for each excitation-energy bin (124 keV wide) was determined from an iterative subtraction technique [19].

From the matrix of primary γ spectra, we have extracted simultaneously the level density and γ-transmission coefficient for ^{56}Fe using the least χ^2 method given in Ref. [20]. The absolute value and slope of the level density were determined from discrete levels [21] below an excitation energy of $E = 4$ MeV and from the comparison to particle-evaporation data [22,23]. To get the absolute value of the γ-transmission coefficient, we used estimated values from systematics (as there are no experimental values) for the neutron-resonance level spacing $D_0 = 2500(1250)$ eV, the total, average γ width $\langle\Gamma_\gamma\rangle = 1500(750)$ meV, and spin cutoff parameters from Ref. [24]. Assuming that dipole radiation dominates the γ decay in the quasicontinuum region, the γSF is deduced from the γ-transmission coefficient by

$$f(E_\gamma) = \mathcal{T}(E_\gamma)/2\pi E_\gamma^3, \tag{1}$$

where $f(E_\gamma)$ is the γSF for γ energy E_γ, and $\mathcal{T}(E_\gamma)$ is the γ-transmission coefficient. The resulting γSFs obtained from the $LaBr_3$ and NaI γ spectra are shown in Fig. 1.

We observe that our new data are in overall very good agreement with the (^{3}He, $\alpha\gamma$) data of Ref. [7]. The upbend is confirmed, using new, higher-resolution detectors and response functions. Also, the different reaction type is expected to populate lower initial spins than the (^{3}He, $\alpha\gamma$) reaction, which has a high cross section for high-ℓ pickup [25]. Compared to the (^{3}He, $\alpha\gamma$) experiment, the particle-detector resolution has been improved from 400 to 90 keV (full width at half maximum), and the

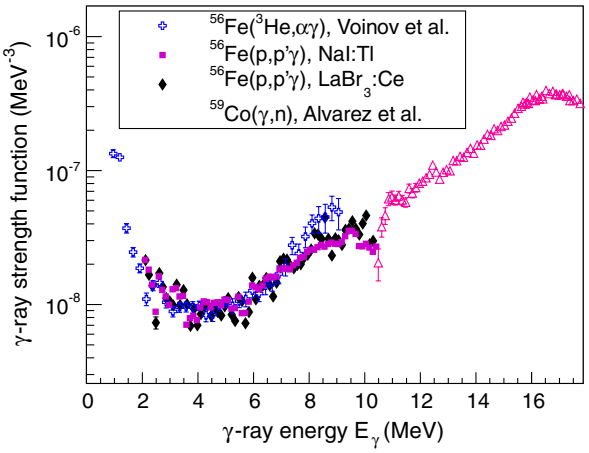

FIG. 1 (color online). Gamma-strength functions of ^{56}Fe from the present experiment and from the (^{3}He, $\alpha\gamma$) data [7] compared with ^{59}Co(γ, n) data from Ref. [26].

γ-energy resolution has been improved by more than a factor of 2 for all γ energies using the $LaBr_3$ crystals. Thus, the upbend is clearly independent from systematic errors in the detector response and reaction-induced effects. The difference in strength at high γ energies might be due to small variations in the normalization of the level density and the new and more precise response functions. Also, we see a good match with photoneutron data on ^{59}Co [26], supporting the chosen values for D_0 and $\langle\Gamma_\gamma\rangle$.

Making use of the various angles for which the NaI detectors were placed, angular distributions were extracted by sorting the data into (E, E_γ) matrices according to the angle θ of the NaI detectors relative to the beam direction. From the intensities as a function of angle, we have fitted angular-distribution functions of the form [27]

$$W(\theta) = A_0 + A_2 P_2(\cos\theta) + A_4 P_4(\cos\theta), \tag{2}$$

where $P_k(\cos\theta)$ is a Legendre polynomial of degree k. The $LaBr_3$ detectors were placed at only four angles and were not used for this analysis, although we note that the shapes of the angular distributions for the $LaBr_3$ and NaI detectors are in very good agreement for the four overlapping angles.

The normalized angular-distribution coefficients are given by $a_k = Q_k \alpha_k A_k / A_0$, where $Q_k \approx 1$ is the geometrical attenuation coefficient due to the finite size of the γ detectors, and α_k is the attenuation due to partial alignment of the nuclei relative to the beam direction. Errors in the intensities are given by $\sigma_{\text{tot}} = \sigma_{\text{stat}} + \sigma_{\text{syst}}$, where the statistical errors are estimated with $\sqrt{N}$ where N is the number of counts, and the systematic errors are deduced from the relative change in N for each symmetric pair of angles (37.4°,142.6°), (63.4°,116.6°), and (79.3°,100.7°). Note that for this high-statistics experiment, the statistical error bars are in general small. However, the systematic uncertainties due to partly asymmetric γ intensities for the pairs

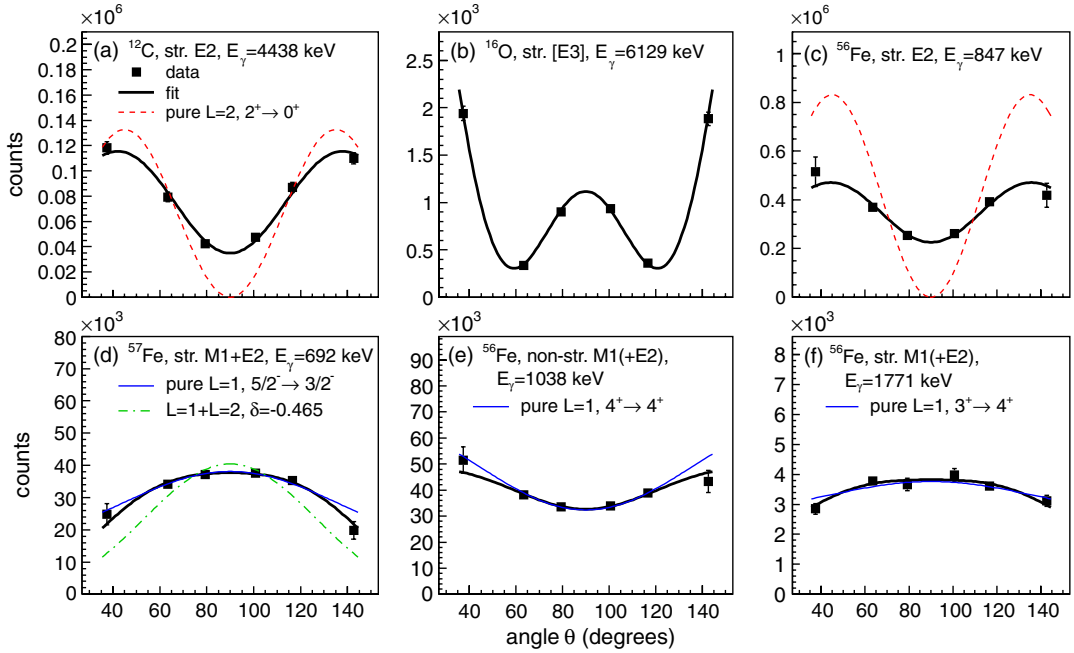

FIG. 2 (color online). Angular distributions of (a) $E2$ in ^{12}C, (b) [$E3$] in ^{16}O, (c) $E2$ in ^{56}Fe, (d) $M1 + E2$ in ^{57}Fe [mixing ratio $\delta = -0.465(8)$ [21], giving an $M1$ fraction of $\approx 82\%$], (e) $M1(+E2)$ in ^{56}Fe, and (f) $M1(+E2)$ in ^{56}Fe. All data (black squares) are measured with the NaI detectors. The thick black lines are Legendre fits; the other lines are theoretical distributions [27] with no attenuation (see the text).

of angles can in some cases be rather large, which in turn influence the uncertainties in the a_k coefficients.

The resulting angular distributions for the 4.4-MeV $E2$ transition in ^{12}C and the 6.1-MeV [$E3$] transition in ^{16}O are shown in Figs. 2(a) and 2(b). Correspondingly, transitions in ^{56}Fe and ^{57}Fe are shown in Figs. 2(c)–2(f). The extracted angular-distribution coefficients are given in Table I. The stretched dipole, quadrupole, and octupole transitions are easily distinguished from each other. We also observe that the attenuation due to partial alignment is becoming less and less pronounced as the excitation energy increases; in fact, the $a_2^{\max}$ coefficients are in good agreement with the data above $E \approx 3$ MeV in ^{56}Fe [see Figs. 2(e) and 2(f)].

We now turn to the distribution of primary γ rays as a function of excitation energy. The matrix of primary γ spectra for ^{56}Fe is displayed in Fig. 3. For γ decay in the quasicontinuum below the neutron threshold, the γSF is dominated by the tail of the GDR. In addition, the giant magnetic dipole resonance (GMDR) typically has its maximum at $E_\gamma = 8$ MeV [28]. Thus, the region of high excitation energy (above $\approx$ 5–6 MeV) is expected to be dominated by dipole transitions.

In the present experiment, the reaction populates a range of initial spins in the quasicontinuum. From the primary transitions, we can clearly identify initial spins up to 6. The angular distributions represent a mix of stretched and non-stretched dipole transitions; if an initial level with spin 4 is populated, it might deexcite with a dipole transition to a final level with spin 3, 4, or 5. Two of these transitions are stretched and one is nonstretched; therefore, one expects that an average of $2/3$ of the transitions is stretched and $1/3$ is nonstretched.

TABLE I. Angular-distribution coefficients of transitions measured in the present experiment (see the text). The theoretical $a_k^{\max}$ coefficients for complete alignment are taken from Ref. [27].

AX	E (keV)	E_γ (keV)	$I_i \to I_f$	XL	$a_2^{\max}$	a_2	$a_4^{\max}$	a_4
^{12}C	4439	4438	$2^+ \to 0^+$	$E2$	0.714	0.55(9)	−1.71	−0.77(13)
^{16}O	6130	6129	$3^- \to 0^+$	[$E3$]	⋯	1.85(8)	⋯	1.91(9)
^{56}Fe	847	847	$2^+ \to 0^+$	$E2$	0.714	0.29(18)	−1.71	−0.60(13)
^{56}Fe	3123	1038	$4^+ \to 4^+$	$M1(+E2)$	0.500	0.31(13)	0.00	−0.09(8)
^{56}Fe	3856	1771	$3^+ \to 4^+$	$M1(+E2)$	−0.167	−0.33(8)	0.00	−0.11(14)
^{56}Fe	4510	3663	$3^- \to 2^+$	$(E1)$	−0.400	−0.31(16)	0.00	0.07(13)
^{56}Fe	5122	3037	$5^- \to 4^+$	$(E1)$	−0.333	−0.42(15)	0.00	0.20(17)
^{57}Fe	706	692	$5/2^- \to 3/2^-$	$M1 + E2$	−1.068	−0.69(12)	0.12	−0.18(9)

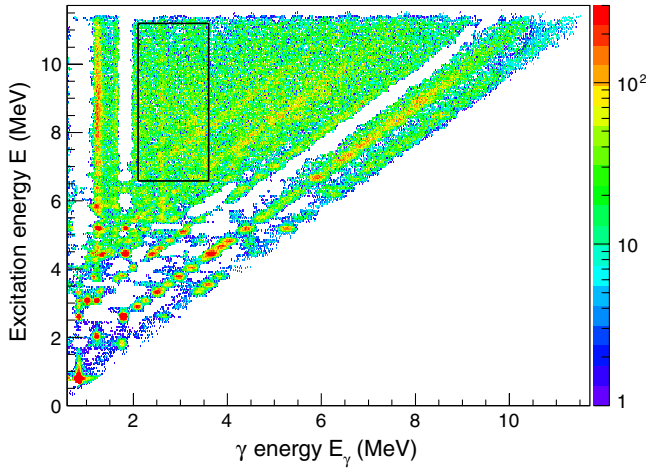

FIG. 3 (color online). Distribution of primary γ rays in ^{56}Fe from the NaI detectors at 79.3°. The box indicates the region used for the angular distributions of $E_\gamma < 3.6$ MeV.

The angular distributions for a nonstretched and a stretched $M1(+E2)$ transition in ^{56}Fe are shown in Figs. 2(e) and 2(f), while in Fig. 4(a), a stretched ($E1$) transition is displayed. The angular distribution of high-energy γ rays for $E > 6.6$ MeV is shown in Fig. 4(b) and for a narrow gate in the region of the upbend in Fig. 4(c), with a shape consistent with a stretched dipole (the exact initial and final spin is unknown). A theoretical distribution assuming a $4 \rightarrow 3$ transition is shown, using values of $a_2^{\max} = -0.357$, $a_4^{\max} = 0.0$ [27], to be compared with the values from the fit $a_2 = -0.35(4)$, $a_4 = -0.10(6)$.

The angular distribution for the whole low-energy region (the box in Fig. 3) is displayed in Fig. 4(d), clearly resembling the high-energy part.

To determine the angular-distribution coefficients for the high-energy γ rays and in the region of the upbend, we have performed independent fits of Eq. (2) to 720-keV-wide excitation-energy slices of the primary γ matrix. Then, a linear fit was performed for all the extracted angular-distribution coefficients, giving $a_2 = -0.07(1)$, $a_4 = -0.09(1)$ and $a_2 = -0.12(3)$, $a_4 = -0.08(3)$ for the low- and high-energy γ rays, respectively (dashed lines in Fig. 4). The a_k coefficients for the two energy regions are compatible within 1σ, which indicates that the nature of these γ rays is very similar. By applying a weight of $2/3$ for the stretched and $1/3$ for the nonstretched known dipole transitions in ^{56}Fe as given in Table I ($E_\gamma = 1038$, 1771, 3037, and 3663 keV), the expected a_k coefficients

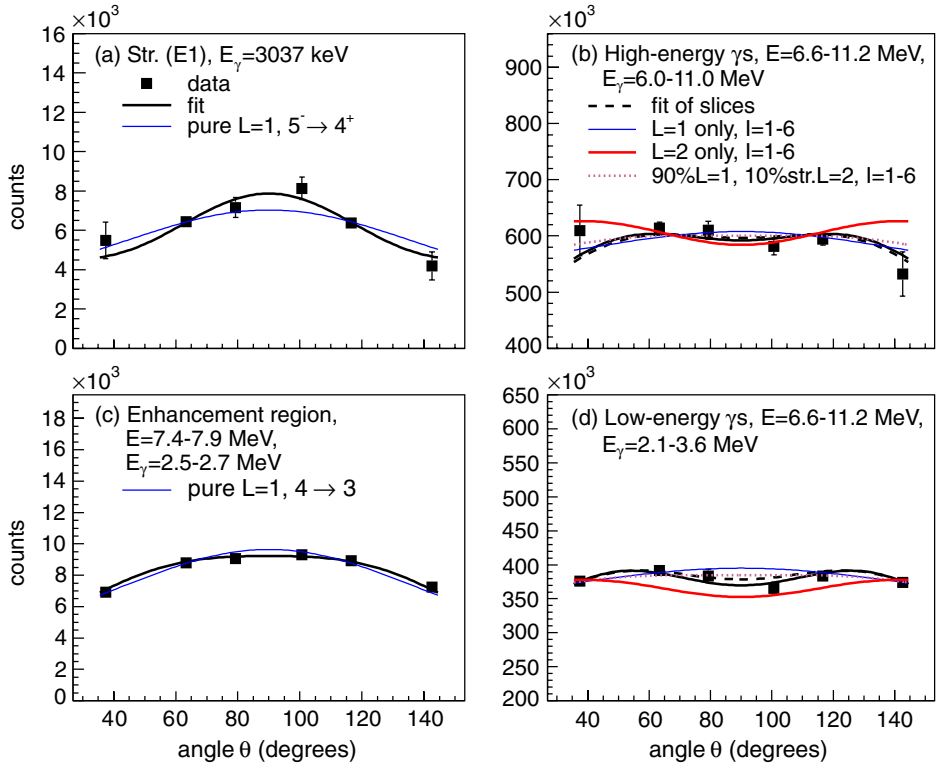

FIG. 4 (color online). Angular distributions from the primary γ matrix of ^{56}Fe: (a) ($E1$) transition, (b) high-energy primary γ rays, (c) narrow E, E_γ gate in the low-energy γ region, and (d) low-energy primary γ rays. The thick black lines show the fit to the data, and the thin blue line gives theoretical dipole distributions. For (b) and (d), the dashed lines show the angular distributions from the fit of many E slices, the blue (red) lines give the theoretical curves for dipole (quadrupole) transitions from initial spins $I_i = 1$–6, and the dotted pink lines are theoretical curves for a mix of $L = 1$ and $L = 2$ transitions (see the text). Note the different scale on the y axis for (b) and (d).

for the quasicontinuum decay are $a_2 = -0.13(7)$ and $a_4 = -0.01(5)$, further supporting that both the low- and high-energy γ regions are dominated by dipole transitions. Based on these findings, we can exclude that the upbend is due to stretched quadrupole ($E2$) or octupole ($E3$) transitions.

We have also considered expected distributions with $a_k^{\max}$ coefficients [27] for an initial spin range $I_i = 1$–6 and final spins $I_f = 0$–7 for stretched and nonstretched dipole transitions, yielding the distribution shown as a blue line in Figs. 4(b) and 4(d). If we assume that there are only quadrupole transitions (stretched and nonstretched, $I_f = 0$–8), the fit is much worse and the data are clearly not reproduced [red lines in Figs. 4(b) and 4(d)]. The best reproduction of the experimental angular distributions was found with a 90% and 10% weight on the dipole and stretched quadrupole contribution ($6 \rightarrow 4$, $5 \rightarrow 3$, $4 \rightarrow 2$, $3 \rightarrow 1$). For an increased weight on the quadrupole contribution, or taking nonstretched and $4 \rightarrow 6, \ldots$ quadrupoles into account, the fit was significantly worse. Therefore, we conclude that $E2$ transitions are of minor importance and that dipole transitions dominate both the region of the upbend and for the high-energy γ's. Our findings support the $L = 1$ assumption applied in Eq. (1).

To summarize, we have presented in this Letter a new measurement on the γ-strength function of ^{56}Fe. The upbend in the strength, which may have profound consequences for r-process reaction rates, is confirmed with an improved detector setup and response functions, and with a different reaction and beam energy. We have demonstrated that the angular distribution of the low-energy primary γ rays is consistent with a mixture of stretched and nonstretched dipole transitions, and that quadrupole and octupole transitions are of minor importance. Thus, for the first time, the multipolarity of the upbend has been measured and shown to exhibit predominantly a dipole character.

A. C. L. gratefully acknowledges funding of this research from the Research Council of Norway, Project Grant No. 205528. M. W. acknowledges support from the National Research Foundation of South Africa. We would like to give special thanks to E. A. Olsen, J. C. Müller, A. Semchenkov, and J. C. Wikne for providing the high-quality beam and excellent experimental conditions.

*a.c.larsen@fys.uio.no

[1] K. Heyde, P. von Neumann-Cosel, and A. Richter, Rev. Mod. Phys. **82**, 2365 (2010).
[2] A. Schiller, A. Voinov, E. Algin, J. A. Becker, L. A. Bernstein, P. E. Garrett, M. Guttormsen, R. O. Nelson, J. Rekstad, and S. Siem, Phys. Lett. B **633**, 225 (2006).
[3] M. Krtička, F. Bečvář, J. Honzátko, I. Tomandl, M. Heil, F. Käppeler, R. Reifarth, F. Voss, and K. Wisshak, Phys. Rev. Lett. **92**, 172501 (2004).
[4] M. N. Harakeh and A. van der Woude, *Giant Resonances* (Oxford University Press, New York, 2001).
[5] S. Goriely, Phys. Lett. B **436**, 10 (1998).
[6] M. Arnould, S. Goriely, and K. Takahashi, Phys. Rep. **450**, 97 (2007).
[7] A. Voinov, E. Algin, U. Agvaanluvsan, T. Belgya, R. Chankova, M. Guttormsen, G. E. Mitchell, J. Rekstad, A. Schiller, and S. Siem, Phys. Rev. Lett. **93**, 142504 (2004).
[8] M. Guttormsen *et al.*, Phys. Rev. C **71**, 044307 (2005).
[9] M. Wiedeking *et al.*, Phys. Rev. Lett. **108**, 162503 (2012).
[10] A. C. Larsen and S. Goriely, Phys. Rev. C **82**, 014318 (2010).
[11] A. Voinov, S. M. Grimes, C. R. Brune, M. Guttormsen, A. C. Larsen, T. N. Massey, A. Schiller, and S. Siem, Phys. Rev. C **81**, 024319 (2010).
[12] E. Litvinova and N. Belov, Phys. Rev. C **88**, 031302(R) (2013).
[13] R. Schwengner, S. Frauendorf, and A. C. Larsen, arXiv:1310.7667 [Phys. Rev. Lett. (to be published)].
[14] M. Guttormsen, A. Bürger, T. E. Hansen, and N. Lietaer, Nucl. Instrum. Methods Phys. Res., Sect. A **648**, 168 (2011).
[15] M. Guttormsen, A. Atac, G. Løvhøiden, S. Messelt, T. Ramsøy, J. Rekstad, T. F. Thorsteinsen, T. S. Tveter, and Z. Zelazny, Phys. Scr. **T32**, 54 (1990).
[16] A. Giaz *et al.*, Nucl. Instrum. Methods Phys. Res., Sect. A **729**, 910 (2013).
[17] R. Nicolini *et al.*, Nucl. Instrum. Methods Phys. Res., Sect. A **582**, 554 (2007).
[18] M. Guttormsen, T. S. Tveter, L. Bergholt, F. Ingebretsen, and J. Rekstad, Nucl. Instrum. Methods Phys. Res., Sect. A **374**, 371 (1996).
[19] M. Guttormsen, T. Ramsøy, and J. Rekstad, Nucl. Instrum. Methods Phys. Res., Sect. A **255**, 518 (1987).
[20] A. Schiller, L. Bergholt, M. Guttormsen, E. Melby, J. Rekstad, and S. Siem, Nucl. Instrum. Methods Phys. Res., Sect. A **447**, 498 (2000).
[21] Data extracted using the NNDC On-Line Data Service from the ENSDF database, August 2013; http://www.nndc.bnl.gov/ensdf/.
[22] A. V. Voinov *et al.*, Phys. Rev. C **74**, 014314 (2006).
[23] H. K. Vonach and J. R. Huizenga, Phys. Rev. **149**, 844 (1966).
[24] T. von Egidy and D. Bucurescu, Phys. Rev. C **80**, 054310 (2009).
[25] R. F. Casten *et al.*, K. Dan. Vidensk. Selsk. Mat. Fys. Medd. **38**, 13 (1972).
[26] R. A. Alvarez, B. L. Berman, D. D. Faul, F. H. Lewis, and P. Meyer, Phys. Rev. C **20**, 128 (1979).
[27] E. der Mateosian and A. W. Sunyar, At. Data Nucl. Data Tables **13**, 391 (1974).
[28] R. Capote *et al.*, Nucl. Data Sheets **110**, 3107 (2009).